ROYAL SOCIETY
OF CHEMISTRY

PAPER

Check for updates

View Article Online
View Journal | View Issue

Improving the luminescence thermal stability of $Ca_3Y_2Ge_3O_{12}$:Cr^{3+} based on cation substitution and its application in NIR LEDs†

Jia Cui,[a] Yibo Zheng,*[b] Zhijun Wang, (ID) *[a] Lingwei Cao,[a] Xuejiao Wang,[a] Yao Yao,[a] Mengya Zhang,[a] Mingjie Zheng,[a] Zhibin Yang[a] and Panlai Li (ID) *[a]

A near-infrared phosphor $Ca_{3-x}Sr_xY_2Ge_3O_{12}$:$Cr^{3+}$ was synthesized by the solid-state method. When Sr^{2+} replaces Ca^{2+}, the thermal stability of the phosphor is obviously improved and the emission intensity at 150 °C can retain 68% of that at room temperature, and its activation energy E_a is 0.331 eV. A novel near-infrared LED was obtained by packaging $Ca_3Y_2Ge_3O_{12}$:$0.01Cr^{3+}$ and a 455 nm blue chip, and the luminescence intensity increased with increasing working current. The results indicate that this phosphor may have a potential application in near-infrared LEDs.

1. Introduction

Near-infrared spectroscopy detection can be used in food and agricultural product detection, pharmacy, biomedicine, and early cancer diagnosis due to its advantages of being simple, fast, real-time and nondestructive, which has attracted the attention of many researchers.[1–6] Common near-infrared light sources are tungsten halide lamps, light-emitting diodes and supercontinuum lasers.[7] Tungsten–halogen lamps suffer from short lifetimes as well as poor efficiency and heat dissipation. Light-emitting diodes normally show narrow emission bands with the largest full width at half maximum (FWHM) of 50 nm.[8,9] Supercontinuum lasers can emit light continuously and are used in spectroscopy; however, their high cost and high power consumption hinder their practical application.[10] At present, an emerging light source that can overcome these obstacles is the combination of blue chips and near-infrared phosphors to obtain a broadband near-infrared LED light source (pc-LED). pc-LED is a promising near-infrared light source due to its tunable fluorescence spectrum, high radiation

flux, small size, simple manufacturing technology, considerable durability and low cost.[11–14] As an important part of pc-LEDs, broadband near-infrared phosphors that can be excited by blue LED chips have become a hot research topic, and their thermal stability is an important parameter to characterize their performance. $LaSc_{2.93}B_4O_{12}$:$0.07Cr^{3+}$ shows an emission band of 700–1200 nm, and its emission intensity at 150 °C is about 30.20% of that at room temperature.[15] When increasing the temperature from 30 to 150 °C, the emission intensity of $ScBO_3$:$0.02Cr^{3+}$ decreases by approximately 51%.[16] The emission intensity at 150 °C of $Ca_3Sc_2Si_3O_{12}$:Cr^{3+} is 54% of that at room temperature.[17] Indeed, in order to meet the application requirements, the temperature stabilities of these materials are another key component; hence, near-infrared phosphors with excellent thermal stability are a problem to be solved.

In a previous work, a series of $Ca_3Y_2Ge_3O_{12}$:Cr^{3+} (CYG:Cr^{3+}) near-infrared phosphors were synthesized by the high temperature solid-state method, and the site occupation and luminescence properties of Cr^{3+} were analyzed in detail. The optimum excitation wavelength was 475 nm, the emission range was 700–1100 nm, and the FWHM was about 155 nm. The results showed that Cr^{3+} replaces Y^{3+} and Ca^{2+}, and the emission intensity of 0.01 Cr^{3+} was the highest among the different Cr^{3+} concentrations.[18] Mao *et al.* also synthesized CYG:Cr^{3+} phosphors and studied their luminescence properties and luminescence thermal stability.[19] Zhao *et al.*[20] and Liu *et al.*[21] reported the cation substitution method to improve the thermal stability of near-infrared luminescence. In order to regulate the luminescence properties of CYG:Cr^{3+} and improve its luminescence thermal stability, the cationic components contained in the $Ca_3Y_2Ge_3O_{12}$ host were regulated. The regulation of host cation components is a common method to realize spectral regulation and optimize performance. The cation

[a] *National-Local Joint Engineering Laboratory of New Energy Photoelectric Devices, Hebei Key Laboratory of Optic-electronic Information and Materials, College of Physics Science & Technology, Hebei University, Baoding 071002, China. E-mail: wangzj1998@126.com, li_panlai@126.com*

[b] *Hebei Key Laboratory of Optoelectronic Information and Geo-detection Technology, Hebei GEO University, Shijiazhuang 050031, China. E-mail: yibo_zheng@126.com*

component may affect the overall crystal field environment. Since Cr^{3+} is easily affected by the crystal field environment, the luminescence performance of Cr^{3+} will change along with the change in the host cation composition. In this work, Sr^{2+} in the same host group was used to control the cation Ca^{2+} in the host based on CYG:Cr^{3+} by adjusting the cation composition of the host. The luminescence thermal stability of the material was improved successfully, and the activation energy and structural rigidity were analyzed in detail.

2. Experimental section

2.1. Preparation of sample

The CSYG:Cr^{3+} samples were synthesized by the high temperature solid-state method. The chemical reagents $CaCO_3$ (99.99%), GeO_2 (99.999%), Y_2O_3 (99.99%), Cr_2O_3 (99.99%) and $SrCO_3$ (99.99%) were used as starting materials. The supplier of these compounds is Zhuzhou Hengma high tech materials Co., Ltd. They were mixed and ground in an agate mortar for more than 30 min to ensure a homogeneous state. Then, the mixtures were transferred to an alumina crucible and heated at 1500 °C for 6 h. Finally, the samples were cooled to room temperature and ground into powder for measurements.

2.2. Material characterization

The phase composition of the samples was determined by X-ray powder diffraction (XRD) analysis, and a Bruker D8 X-ray diffractometer with Ni-filtered Cu Kα radiation (λ = 0.15405 nm)

operating at 40 mA, 40 kV was used for the measurements at a step length of 0.05° and diffraction range of 10°–80°. The software Find it, the general structure analysis system (GSAS) program, and Crystalmaker were used to determine the phase information. The spectral property and luminescence decay curves of the samples were determined using a FLS920 (Edinburgh Instruments) fluorescence spectrometer. To verify the valence state of Cr^{3+} ions, the samples were tested using an X-ray photoelectron spectrometer with the model AXIS ULTRADLD.

3. Results and discussion

3.1. Phase formation and structural analysis

The crystal structure and the local coordination of the Ca^{2+}, Y^{3+} and Ge^{4+} sites are shown in Fig. 1(a). CYG possesses a garnet structure, with a cubic structure and a space group of $Ia\bar{3}d$. Since the luminescence intensity of CYG:0.01Cr^{3+} is the highest among the different Cr^{3+} concentrations, the luminescence thermal stability of CYG:0.01Cr^{3+} is further studied. The structure is composed of a calcium–oxygen dodecahedron, an yttrium–oxygen octahedron and a germanium–oxygen tetrahedron. Fig. 1(b) depicts the XRD characterization of all the CSYG:001Cr^{3+} samples and the diffraction peaks are in good agreement with PDF#040114317. The results show that all the samples are pure phase. In order to study the changes of the cell volume and cell parameters of the sample, the Rietveld refinements of the XRD profile were performed for the CSYG:001Cr^{3+} samples using the

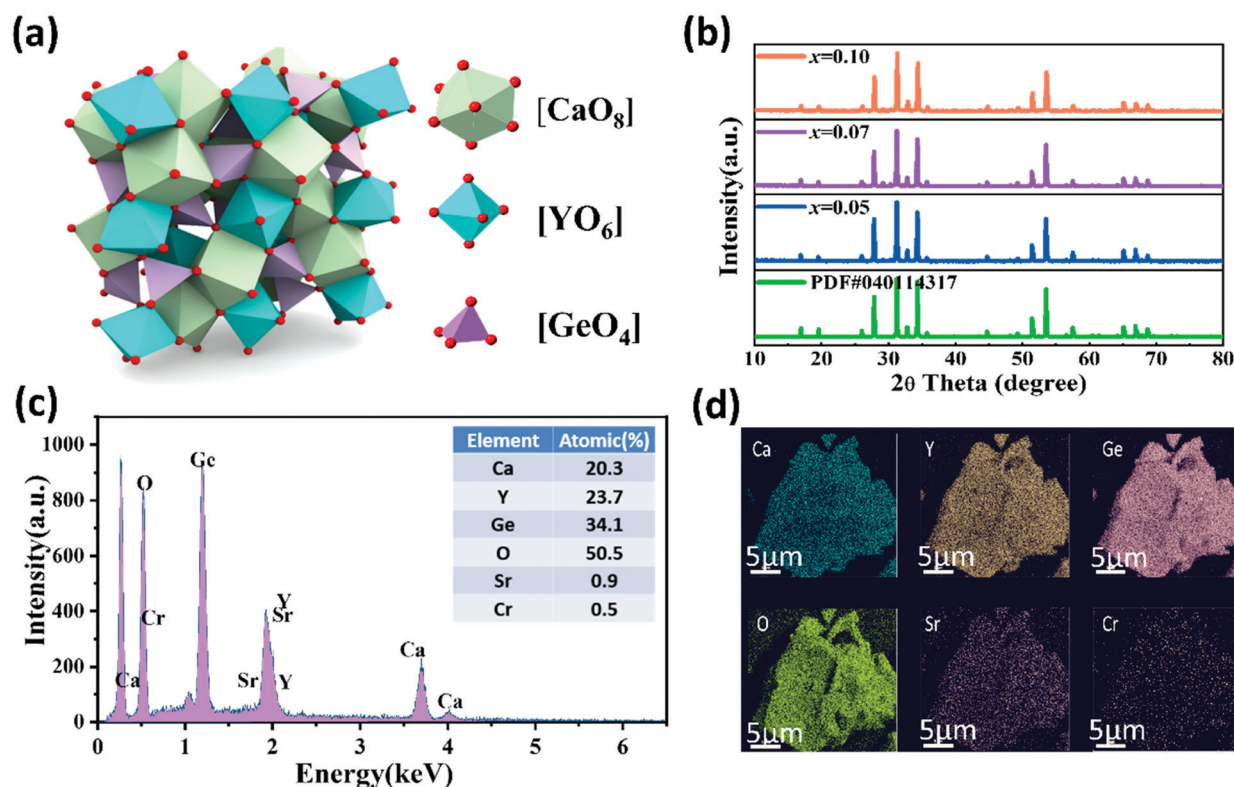Fig. 1 (a) The crystal structure of CYG. (b) The XRD patterns of $C_{3-x}S_xYG$:0.01Cr^{3+}(x = 0.05, 0.07, 0.10) and the standard data of the CYG phase (PDF#040114317). (c and d) The EDS and elemental mapping of $C_{2.93}S_{0.07}YG$:0.01Cr^{3+}.

general structure analysis system (GSAS) program, and the results are given in Fig. S1 (ESI†). According to the refined data, when the Sr^{2+} concentration is increased, the cell volume V and cell parameter $a/b/c$ show a gradual increasing trend, which is due to the fact that the large radius Sr^{2+} ($r = 1.26$ Å, $N = 8$) replaces the smaller radius Ca^{2+} ($r = 1.12$ Å, $N = 8$). The results are shown in Fig. S2(a) (ESI†). Since $[CaO_8]$ and $[YO_6]$ are connected through a common edge, the expansion of the $[CaO_8]$ lattice squeezes $[YO_6]$, and the volume of $[YO_6]$ is thus slightly reduced, as shown in Fig. S2(b) (ESI†). The EDS spectrum is shown in Fig. 1(c), from which we can see the types and contents of the elements in the sample. From the elemental mapping images of the sample in Fig. 1(d), it can be seen that Ca, Y, Ge, O, Cr and Sr are homogeneously distributed throughout the particles without any traceable elemental aggregation or phase separation.

3.2. Luminescence properties of $C_{3-x}S_xYG$:0.01Cr^{3+}

The emission spectra of $C_{3-x}S_xYG$:0.01Cr^{3+} with different concentrations of Sr^{2+} under an excitation of 475 nm are shown in Fig. S3 (ESI†). The emission intensity of Cr^{3+} increases gradually with the increase of Sr^{2+} content. When $x = 0.07$, the emission intensity is the strongest, and is about twice the original initial intensity. The structure rigidity of the host will affect the emission intensity of the activated ions. With the increase of the rigidity, the emission intensity will increase.[22] The change of structural rigidity with varying Sr^{2+} content will be discussed in the present work.

In order to analyze the effect of Sr^{2+} on the thermal stability of CYG:Cr^{3+}, the emission spectra of samples with different temperatures were measured, and the results are shown in Fig. 2(a–d). The temperature range is 25–150 °C and the excitation wavelength is 475 nm. It can be seen from the spectra that the emission intensity of the samples decreases continuously when the temperature rises from room temperature to 150 °C. Fig. 3(a) presents that, at $x = 0.07$, the emission intensity of the sample shows the slowest decrease with increasing temperature. As the temperature increases to 150 °C, the relative integrated emission intensity remains at about 68%. The emission intensities of the samples with $x = 0.05$ and 0.10 are 53% and 31% of the initial intensity at 150 °C, respectively. For $x = 0$, the emission intensity of the sample decreases the most rapidly with increasing temperature. One of the key parameters to characterize the luminescence thermal stability of materials is the activation energy E_a. In general, the greater the value of the activation energy, the better the luminescence thermal stability of the material, and the value of the activation energy E_a can be calculated using the Arrhenius equation:[23–26]

$$I_T = \frac{I_0}{1 + c \exp\left(-\dfrac{\Delta E}{kT}\right)} \tag{1}$$

In this expression, k is the Boltzmann constant, I_0 and I_T are the emission intensities of the sample at room temperature and
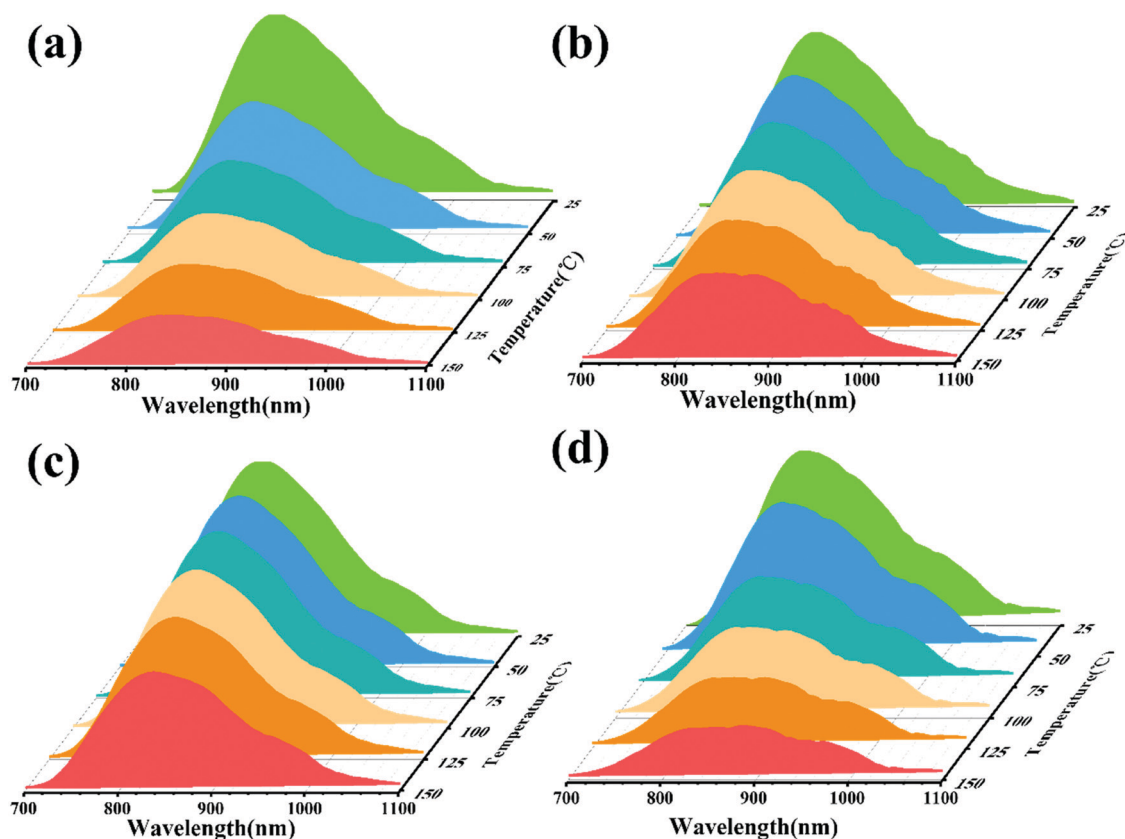

Fig. 2 (a–d) Temperature spectrum of $C_{3-x}S_xYG$:0.01Cr^{3+} ($x = 0$, 0.05, 0.07, and 0.10, respectively) ($\lambda_{ex} = 475$ nm).
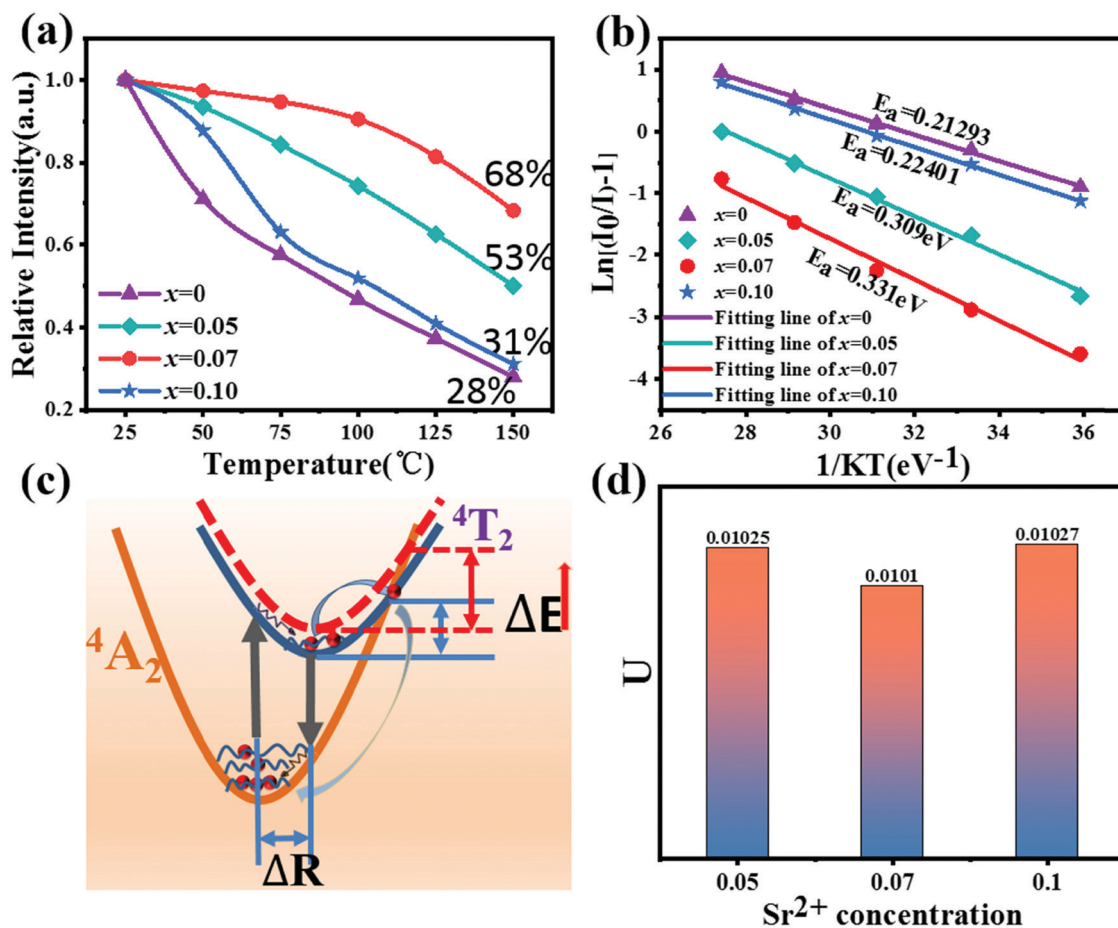
Fig. 3 (a) Temperature-dependent normalized integrated intensities of $C_{3-x}S_xYG:0.01Cr^{3+}$ ($x = 0, 0.05, 0.07, 0.10$). (b) Fitting curve of the activation energy of $C_{3-x}S_xYG:0.01Cr^{3+}$($x = 0, 0.05, 0.07, 0.10$). (c) The configuration coordinate diagram. (d) Atomic displacement parameter U of $C_{3-x}S_xYG:0.01Cr^{3+}$($x = 0, 0.05, 0.07, 0.10$).

a specific temperature, respectively, ΔE is the activation energy of thermal quenching, and T is the specific temperature.

The relationship between $1/KT$ and $\ln[(I_0/I) - 1]$ is obtained by processing the spectral data, and a straight line is obtained
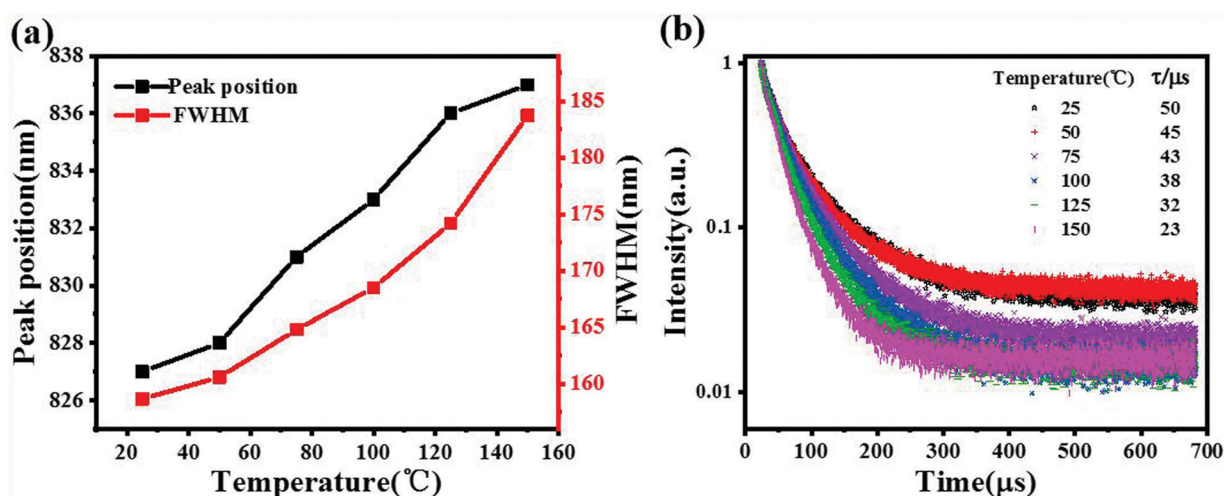

Fig. 4 (a) The half peak width and peak position of $C_{2.93}S_{0.07}YG:0.01Cr^{3+}$ with temperature. (b) Fluorescence decay curves of $C_{2.93}S_{0.07}YG:0.01Cr^{3+}$ at different temperatures.

by linear fitting. The activation energy E_a is the absolute value of the slope of the straight line. The activation energies of these samples are $E_a(x = 0.07) = 0.331$ eV, $E_a(x = 0.05) = 0.309$ eV, $E_a(x = 0.10) = 0.224$ eV, and $E_a(x = 0) = 0.213$ eV. When $x = 0.07$, the sample shows the best luminescence thermal stability and the maximum activation energy. As the activation energy E_a increases, it becomes more difficult for the activated electrons to overcome the energy barrier; hence, the influence of non-radiative transition is reduced, and the thermal stability is improved. The enhancement mechanism is shown in the configuration diagram in Fig. 3(c), and the thermal stability energy of the material is related not only to the activation energy but also to the Stokes shift ΔR, which is usually related to the degree of lattice structure rigidity.[27–30] George et al.[31,32] and Brgoch et al.[33] took the Debye temperature as a parameter to characterize rigidity of the lattice structure. For the same host, the higher the Debye temperature, the better the structural rigidity. The formula of the Debye temperature Θ_D is as follows:

$$\Theta_{D,i} = \sqrt{\frac{3\hbar^2 T N_A}{A_i k_B U_{iso,i}}} \quad (2)$$

where i is the type of atom, A_i is the mass of the atom and U_{iso} is the displacement parameter of the atom. It can be seen from the formula that the Debye temperature is inversely proportional to the atomic displacement parameter. According to the refined data, the atomic displacement parameters of $x = 0.05$, 0.07 and 0.10 can be calculated, as shown in Fig. 3(d). When $x = 0.07$, the value of U_{iso} is the lowest, that is, it has a higher Debye temperature and the highest degree of rigidity, and hence the sample has better luminescence thermal stability.

The thermal quenching behavior includes not only the change of emission intensity but also the change of emission peak position and half peak width with increasing temperature. The $x = 0.07$ sample with the best luminescence thermal stability was selected. With the increase in temperature, the

change of the emission peak position and half peak width of the sample can be seen in Fig. 4(a). During the transition from room temperature to high temperature, the emission spectra of the samples shifted about 10 nm towards the long wave direction, and the half-peak width widened by about 25 nm. The red shift of the spectra with increasing temperature can be explained by the Varshini formula[34]

$$E(T) = E_0 - \frac{aT^2}{T + b} \quad (3)$$

where $E(T)$ is the energy difference between the ground state and the excited state at the corresponding temperature, $E(0)$ is the energy difference at $T = 0$ K, and a and b are lattice-related parameters. When the temperature increases, the energy difference $E(T)$ will decrease, that is, the energy produced by the photon transition from the excited state to the ground state will decrease, resulting in a red shift. At the same time, with the increase in temperature, the lattice expands to a certain extent, leading to an increase in the bond length and the weakening of the crystal field strength around Cr^{3+}, which leads to the red shift of the emission band.[35] The relationship between the FWHM of the emission peak and temperature is as follows:[36]

$$FWHM(T) = W_0 \sqrt{\coth\left(\frac{hw}{2kt}\right)} \quad (4)$$

$$W_0 = \sqrt{8\ln 2}(hw)\sqrt{s} \quad (5)$$

where k represents the Boltzmann constant, S is the Huang–Rhys–Pekar parameter, W_0 shows the value of the FWHM at 0 K and hw represents the energy of the lattice vibration. From the above formula, it can be seen that the FWHM depends largely on the lattice vibration (hw). With the increase in temperature, the crystal structure of the material becomes looser, which will cause larger lattice vibration and widen the half peak width. In addition, with the increase in temperature, the electron phonon interaction will gradually enhance, resulting in the
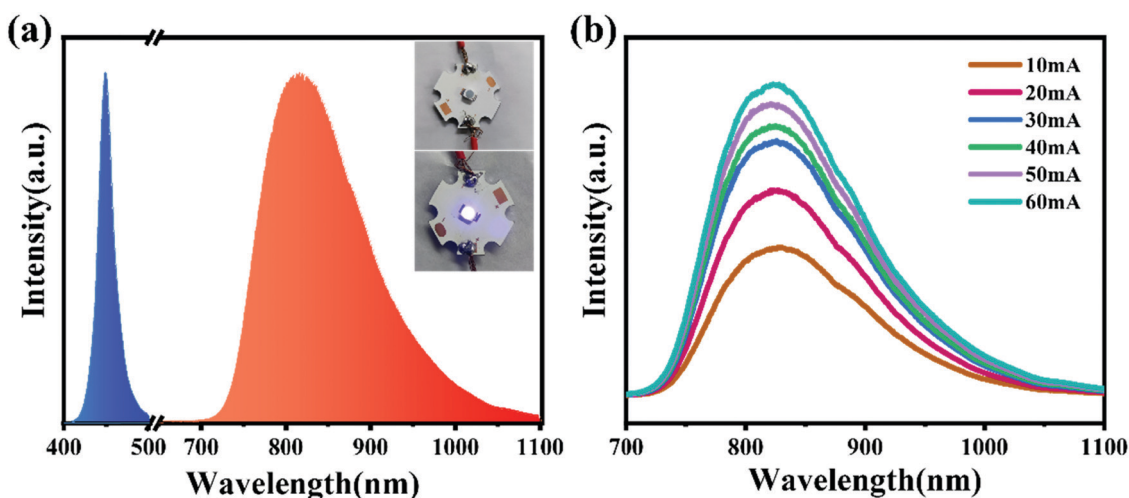

Fig. 5 (a) Electroluminescence spectrum and photograph of the fabricated NIR LED (CSYG:0.01Cr^{3+} + 455 nm LED chip; voltage of 3.0 V and current of 11 mA). (b) Luminescence spectra as a function of work current.

widening of the FWHM.[37,38] To further investigate the thermal quenching behavior, the fluorescence decay curves of the sample were measured with the increase in temperature, and the results are shown in Fig. 4(b). The fluorescence decay curves can be fitted with the second-order exponential function, and the expression of the second-order exponential function is:[39–41]

$$I_{(t)} = I_0 + A_1 e^{-t/\tau_1} + A_2 e^{-t/\tau_2} \qquad (6)$$

In the above expression, $I_{(t)}$ is the luminous intensity, A_1 and A_2 are constants, t is the decay time, and τ_1 and τ_2 are the lifetimes of fast and slow decay, respectively. The average decay time τ^* can be calculated by the formula:

$$\tau^* = \left(A_1\tau_1^2 + A_2\tau_2^2\right)/\left(A_1\tau_1 + A_2\tau_2\right) \qquad (7)$$

The lifetime of the sample from normal temperature to high temperature can be obtained using the above formula. With the increase in temperature, the lifetime of the sample decreased from 50 μs to 23 μs. The reason for this phenomenon is that the non-radiative transition increases gradually with the increase in temperature, which leads to the decrease of the fluorescence lifetime of the activated ions.

3.3. Applications in NIR LEDs

A NIR LED was fabricated with CYG:0.01Cr^{3+} on a 455 nm LED chip under a voltage of 3.0 V and current of 11 mA, whose electroluminescence (EL) spectrum and photograph are shown in Fig. 5a. As a comparison, the EL spectra of the NIR LED with different work currents are depicted in Fig. 5b, and the results indicate that the luminescence intensity can be enhanced by increasing the work current. The results show that this phosphor may be applicable in NIR LEDs.

4. Conclusions

In this work, the emission intensity at 150 °C compared to that at room temperature increased from 28% to 68% by introducing larger radius Sr^{2+} to adjust Ca^{2+} in the host. The enhancement of the thermal stability of the material occurs since the activation energy of the material increases due to the introduction of Sr^{2+}, which reduces the influence of non-radiative transition. At the same time, the rigidity of the material structure increases, which is one of the important factors to enhance the thermal stability. A NIR LED can be fabricated by combining CYG:0.01Cr^{3+} and a 455 nm LED chip. The results indicate that this phosphor may be used in NIR LEDs.

Conflicts of interest

The authors declare that they have no conflicts of interest.

Acknowledgements

References

1 P. A. Martin, Near-infrared diode laser spectroscopy in chemical process and environmental air monitoring, *Chem. Soc. Rev.*, 2002, **31**(4), 201–210.

2 M. Blanco and I. Villarroya., NIR spectroscopy: a rapid-response analytical tool, *TrAC, Trends Anal. Chem.*, 2002, **21**(4), 240–250.

3 R. Usamentiaga, P. Venegas and J. Guerediaga, *et al.*, Infrared thermography for temperature measurement and non-destructive testing, *Sensors*, 2014, **14**(7), 12305–12348.

4 M. H. Fang, P. Y. Huang and Z. Bao, *et al.*, Penetration in biological tissue using light-emitting diodes with highly efficient near-infrared ScBO$_3$:Cr^{3+} phosphor, *Chem. Mater.*, 2020, **32**(5), 2166–2171.

5 H. Suo, X. Q. Zhao and Z. Y. Zhang, *et al.*, Ultra sensitive optical nano thermometer LaPO$_4$:Yb^{3+}/Nd^{3+} based on thermo-enhanced NIR to NIR emission, *Chem. Eng. J.*, 2020, 124506.

6 S. S. Ding, H. J. Guo and P. Feng, *et al.*, A new near-infrared long persistent luminescence material with its outstanding persistent luminescence performance and promising multifunctional application prospects, *Adv. Opt. Mater.*, 2020, 2000097.

7 V. Rajendran, M. H. Fang and G. N. D. Guzman, *et al.*, Super broadband near-infrared phosphors with high radiant flux as future light sources for spectroscopy applications, *ACS Energy Lett.*, 2018, **3**, 2679–2684.

8 C. B. Han, C. He and X. J. Li., Near-infrared light emission from a GaN/Si nanoheterostructure array, *Adv. Mater.*, 2011, **23**(41), 4811–4814.

9 H. Bechtel, P. J. Schmidt, A. Tücks, *et al.*, *Fully phosphor-converted LEDs with Lumiramic phosphor technology*. Tenth International Conference on Solid State Lighting. International Society for Optics and Photonics, 2010, **7784**, 77840W.

10 D. Hayashi, A. M. V. Dongen and J. Boerekamp, *et al.*, A broadband LED source in visible to short-wave-infrared wavelengths for spectral tumor diagnostics, *Appl. Phys. Lett.*, 2017, **110**(23), 233701.

11 V. Rajendran, H. Chang and R. S. Liu, Recent progress on broadband near-infrared phosphors-converted light emitting diodes for future miniature spectrometers, *Opt. Mater.: X*, 2019, **1**, 100011.

12 V. Rajendran, T. Lesniewski and S. Mahlik, *et al.*, Ultra-broadband phosphors converted near-infrared light emitting diode with efficient radiant power for spectroscopy applications, *ACS Photonics*, 2019, **6**, 3215–3224.

13 L. L. Zhang, Cr^{3+} doped broadband near infrared phosphors and their research progress, *J. Lumin.*, 2019, **40**(12), 11.

14 J. M. Wu, Luminescence and device properties of Cr^{3+} and Yb^{3+} Co doped LaSc$_3$(BO$_3$)$_4$ near infrared phosphors, *J. Lumin.*, 2021, **42**(06), 793–803.

15 T. Y. Gao, W. D. Zhuang and R. H. Liu, *et al.*, Design of a broadband NIR phosphor for security-monitoring LEDs: Tunable photoluminescence properties and enhanced thermal stability, *Cryst. Growth Des.*, 2020, **6**, 3851–3860.

16 Q. Y. Shao, D. Hao and L. Q. Yao, *et al.*, Photoluminescence properties of a $ScBO_3:Cr^{3+}$ phosphor and its applications for broadband near-infrared LEDs, *RSC Adv.*, 2018, **8**(22), 12035–12042.

17 Z. W. Jia, C. X. Yuan and R. Y. Li, *et al.*, Electron-phonon coupling mechanisms of broadband near-infrared emissions from Cr^{3+} in the $Ca_3Sc_2Si_3O_{12}$ garnet, *Phys. Chem. Chem. Phys.*, 2020, **22**(18), 10343–10350.

18 J. Cui, P. L. Li and L. W. Cao, *et al.*, Achievement of broadband near-infrared phosphor $Ca_3Y_2Ge_3O_{12}:Cr^{3+}$, Ce^{3+} *via* energy transfer for food analysis, *J. Lumin.*, 2021, **237**, 118170.

19 N. Mao, S. Liu and Z. Song, *et al.*, A Broadband Near-Infrared Phosphor $Ca_3Y_2Ge_3O_{12}:Cr^{3+}$ with Garnet Structure[J], *J. Alloys Compd.*, 2021, **863**, 158699.

20 F. Zhao, H. Cai and S. Zhang, *et al.*, Octahedron-dependent near-infrared luminescence in Cr^{3+}-activated phosphors, *Mater. Today Chem.*, 2022, **23**, 10074.

21 S. Liu, H. Cai and S. Zhang, *et al.*, Site engineering strategy toward enhanced luminescence thermostability of a Cr^{3+}-doped broadband NIR phosphor and its application[J], *Mater. Chem. Front.*, 2021, **5**, 3841–3849.

22 W. Wang, H. Yang and Y. X. Liu, *et al.*, Photoluminescence control and abnormal Eu^{3+} orange emission in Ln^{3+} (Ln^{3+} = Ce^{3+}, Eu^{3+})-doped oxyapatite-type phosphors, *CrystEngComm*, 2019, **22**(2), 311–319.

23 S. P. Lee, T. S. Chan and T. M. Chen, *et al.*, Novel reddish-orange-emitting $BaLa_2Si_2S_8$: Eu^{2+} thiosilicate phosphor for LED lighting, *ACS Appl. Mater. Interfaces*, 2014, **7**(1), 40–44.

24 Q. Q. Wang, S. Y. Zhang and Z. W. Li, *et al.*, Near infrared-emitting Cr^{3+}/Eu^{3+} co-doped zinc gallogermanate persistence luminescent nanoparticles for cell imaging, *Nanoscale Res. Lett.*, 2018, **13**(1), 64.

25 R. J. Xie, N. Hirosaki and N. Kimura, *et al.*, 2-phosphor-converted white light-emitting diodes using oxynitride/nitride phosphors, *Appl. Phys. Lett.*, 2007, **90**, 191101.

26 Z. Xia, X. Wang and Y. Wang, *et al.*, Synthesis, structure, and thermally stable luminescence of Eu^{2+}-doped $Ba_2Ln(BO_3)_2Cl$ (Ln = Y, Gd and Lu) host compounds, *Inorg. Chem.*, 2011, **50**, 10134–10142.

27 G. Blasse and B. C. Grabmaier, *Luminescent Materials*, Springer-Verlag, Berlin, 1994.

28 T. Y. Gao, W. D. Zhuang and R. H. Liu, *et al.*, Design of a Broadband NIR Phosphor for Security-Monitoring LEDs: Tunable Photoluminescence Properties and Enhanced Thermal Stability[J], *Cryst. Growth Des.*, 2020, **20**(6), 3851–3860.

29 J. C. Zhang, J. L. Zhang and W. L. Zhou, *et al.*, Composition screening in blue-emitting $Li_4Sr_{1+x}Ca0.9_{7-x}(SiO_4)_2$: Ce^{3+} phosphors for high quantum efficiency and thermal stable photoluminescence, *ACS Appl. Mater. Interfaces*, 2017, **9**, 30746–30754.

30 Y. N. Zhou, W. D. Zhuang and Y. S. Hu, *et al.*, Second-sphere polyhedron distortion induced broadened and red-shifted emission in $Lu_3(Mg_xAl_{2-x})(Al_{3-x}Si_x)O_{12}:Ce^{3+}$ for Warm W-LED, *Inorg. Chem.*, 2019, **58**, 9108–9117.

31 N. C. George, A. Birkel and J. Brgoch, *et al.*, Average and local structural origins of the optical properties of the nitride phosphor $La_{3-x}Ce_xSi_6N_{11}$ ($0 < x \le 3$), *Inorg. Chem.*, 2013, **52**(23), 13730–13741.

32 N. C. George, A. J. Pell and G. Dantelle, *et al.*, Local environments of dilute activator ions in the solid-state lighting phosphor $Y_{3-x}Ce_xAl_5O_{12}$, *Chem. Mater.*, 2013, **25**(20), 3979–3995.

33 J. Brgoch, S. P. DenBaars and R. Seshadri, Proxies from *Ab initio* calculations for screening efficient Ce^{3+} phosphor hosts, *J. Phys. Chem. C*, 2013, **117**(35), 17955–17959.

34 J. S. Kim, Y. H. Park and S. M. Kim, *et al.*, Temperature-dependent emission spectra of M_2SiO_4: Eu^{2+} (M = Ca, Sr, Ba) phosphors for green and greenish white LEDs, *Solid State Commun.*, 2005, **133**(7), 445–448.

35 X. X. Xu, Q. Y. Shao and L. Q. Yao, *et al.*, Highly efficient and thermally stable Cr^{3+}-activated silicate phosphors for broadband near-infrared LED applications, *Chem. Eng. J.*, 2020, **383**, DOI: 10.1016/j.cej.2019.123108.

36 Y. Wang, J. Ding and Y. Wang, *et al.*, Structural design of new $Ce^{3+}/Eu2+$-doped or co-doped phosphors with excellent thermal stabilities for WLEDs[J], *J. Mater. Chem. C*, 2019, **7**, DOI: 10.1039/c8tc06013d.

37 S. Liu, Z. Wang, H. Cai and Z. Song, *et al.*, Highly efficient near-infrared phosphor $LaMgGa_{11}O_{19}:Cr^{3+}$, *Inorg. Chem. Front.*, 2020, **7**(6), 1467–1473.

38 Z. Jia, C. Yuan and Y. Liu, *et al.*, Strategies to approach high performance in Cr^{3+}-doped phosphors for high-power NIR-LED light sources[J], *Light: Sci. Appl.*, 2020, **9**(1), 86.

39 K. Li, M. Xu and J. Fan, *et al.*, Tunable green to yellowish-orange phosphor $Na_3LuSi_2O_7$: Eu^{2+}, Mn^{2+} via energy transfer for UV-LEDs, *J. Mater. Chem. C*, 2015, **3**(44), 11618–11628.

40 K. Li, J. Xu and X. Cai, *et al.*, An efficient green-emitting α-$Ca_{1.65}Sr_{0.35}SiO_4$: Eu^{2+} phosphor for UV/n-UV w-LEDs: synthesis, luminescence and thermal properties, *J. Mater. Chem. C*, 2015, **3**(24), 6341–6349.

41 M. Yu, J. Lin and J. Fang, Silica spheres coated with $YVO_4:Eu^{3+}$ layers via sol-gel process: a simple method to obtain spherical core-shell phosphors, *Chem. Mater.*, 2005, **17**, 1783–1791.